Absorption and injection models for open time-dependent quantum systems

F. L. Traversa,[*] Z. Zhan,[†] and X. Oriols[‡]
Departament d'Enginyeria Electrònica, Universitat Autònoma de Barcelona, 08193-Bellaterra (Barcelona), Spain
(Received 27 May 2014; published 11 August 2014)

In the time-dependent simulation of pure states dealing with transport in open quantum systems, the initial state is located outside of the active region of interest. Using the superposition principle and the analytical knowledge of the free time evolution of such a state outside the active region, together with absorbing layers and remapping, a model for a very significant reduction of the computational burden associated with the numerical simulation of open time-dependent quantum systems is presented. The model is specially suited to study (many-particle and high-frequency effects) quantum transport, but it can also be applied to any other research field where the initial time-dependent pure state is located outside of the active region. From numerical simulations of open quantum systems described by the (effective mass) Schrödinger and (atomistic) tight-binding equations, a reduction of the computational burden of about two orders of magnitude for each spatial dimension of the domain with a negligible error is presented.

DOI: 10.1103/PhysRevE.90.023304 PACS number(s): 02.60.Cb, 73.63.−b, 02.60.Lj, 72.10.Bg

I. INTRODUCTION

The ultimate reason why the quantum theory gives rise to a host of puzzling and fascinating phenomena (without classical counterpart) is because quantum states live in a high-dimensional and abstract configuration space [rather than in the ordinary three-dimensional (3D) physical space]. The computational burden associated with the N-particle state makes the exact solution of the many-particle Schrödinger equation inaccessible in most practical situations. Historically, among other strategies, the computational burden has been reduced by selecting Hamiltonian eigenstate as the representation of particles. For example, the (lowest-energy) ground state successfully explains the behavior of equilibrium quantum systems.

However, there are many quantum scenarios in which the time-dependent Schrödinger equation needs to be explicitly considered [1]. For example, when light intensity is sufficiently small, a first-order time-independent perturbative theory is enough to describe the main features of the interaction between light and matter, but when the light intensity becomes larger, a plethora of different phenomena appears and more accurate models are required. The exact quantum description of the photoionization due to the interaction of an atom (or molecule) with a (classical) electromagnetic pulse in the nonrelativistic regime is the time-dependent Schrödinger equation [2–6]. Equivalently, the quantum transport in mesoscopic systems has been mainly understood from (time-independent) scattering states [7,8]. However, strictly speaking, the scattering states do not belong to the *physical* states of any Hilbert space because they cannot be normalized to unity. In other words, strictly speaking, these states cannot be associated with an electron localized at the right or left of the device-active region because they extend everywhere, at any time [9]. Certainly, these Hamiltonian eigenstates can be used as a basis to define well-localized electrons by superposition. However, a proper superposition of eigenstates can only be useful numerically to describe the evolution of wave packets in time-independent Hamiltonians (where eigenstates remain invariant with time). Any time-dependent potential requires an explicit solution of the time-dependent Schrödinger equation.

The need for time-dependent algorithms to properly understand quantum transport has already been discussed in the literature in several different contexts. For example, the time-independent density functional theory is said to be unable to properly capture nonequilibrium scenarios, while time-dependent versions are mandatory for successful predictions [10–13]. Similarly, in quantum transport, it is said that the Landauer formula is incomplete because one-particle scattering probabilities do not capture the many-body effects [14]. In the same way, there are many difficulties in treating ac and transient dynamics properly using time-independent pictures [15–17]. Additionally, the advantages of modeling transport in waveguides using wave packets have also been indicated [1,2,18,19]. We have also shown quite recently that the Bohmian conditional wave function is a very powerful tool to deal with both quantum many-body problems and nonunitary evolutions [16,20], and it is useful to simulate ac and transient current as well as noise in mesoscopic devices [21,22]. By constructions, such (Bohmian conditional) wave functions also require a time-dependent evolution.

A. Problem setting

The main motivation of the present work is to reduce the computational burden associated with the study of quantum transport with time-dependent pure states. As we will see, the computation of quantum transport has some peculiarities that imply new and unexplored methods to greatly simplify the numerical computational resources. A general scenario for modeling quantum transport assumes a finite domain Ω where the time-dependent wave function is solved [see Fig. 1(a)]. Such a domain contains a flat potential region except in the interaction box Ω', i.e., the so-called active region, where the potential V can be time-dependent and inhomogeneous. By construction, the support of the time-dependent wave function, at long times, can be located very far from the

[*]fabio.traversa@polito.it
[†]zhenzhanh@gmail.com
[‡]xavier.oriols@uab.es

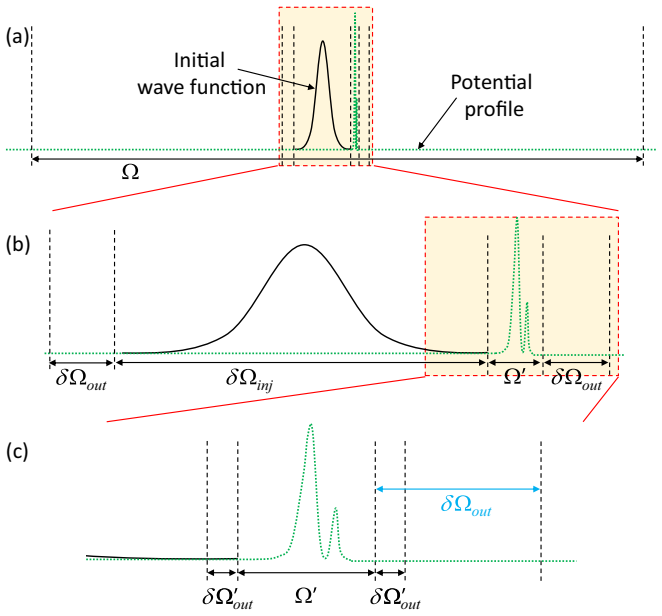

FIG. 1. (Color online) Spatial simulation domains. (a) *Infinite domain*: the full domain Ω is a large enough domain to avoid interactions with boundaries during the simulation time. (b) *Absorbing layers*: reduced domain $\delta\Omega_{\text{out}} \cup \delta\Omega_{\text{inj}} \cup \Omega' \cup \delta\Omega_{\text{out}}$ using standard absorbing algorithms, where $\delta\Omega_{\text{inj}}$ is the layer for the injection, i.e., the layer that includes the wave function at the initial time, Ω' is the interaction box, and $\delta\Omega_{\text{out}}$ at both sides are the absorbing layers. (c) *Absorbing layers plus analytical injection*: further reduced domain $\delta\Omega'_{\text{out}} \cup \Omega' \cup \delta\Omega'_{\text{out}}$ presented in this work; it has no need for an injection layer, and it employs smaller absorbing layers $\delta\Omega'_{\text{out}} \ll \delta\Omega_{\text{out}}$ obtained exploiting a change of coordinates (remapping).

interaction box Ω', therefore to eliminate spurious events at the boundaries, Ω is generally selected to be extremely large. Thus, in order to avoid the very large domain of Fig. 1(a), several absorbing boundary conditions have been developed for the time-dependent Schrödinger equation (see [23,24] and references therein). Some approaches are based, for example, either on fitting the wave function to plane waves at the boundaries [25,26], or on time convolution integrals at the boundaries to construct a transparent boundary condition [27–30]. If this approximate solution actually coincides on Ω' with the exact solution of the whole-space problem, one refers to these boundary conditions as transparent boundary conditions [23]. However, such conditions require an increment of the complexity in the computer implementation due to their formulation employing spatial and time-convolution integrals. Other much simpler strategies that provide a negligible error when compared to the transparent boundary conditions are greatly preferred. One common strategy of this second type is the use of absorption or attenuation layers $\delta\Omega_{\text{out}}$ at the boundaries of the simulation domain [24,31–33], as depicted in Fig. 1(b). The value of the wave function at $\delta\Omega_{\text{out}}$ is decreased at each time step of the simulation. This idea can also be interpreted as an application of the exterior complex scaling [33] as well as adding an artificial complex potential at $\delta\Omega_{\text{out}}$ [24,31] (see Appendix A). Let us notice, however, that this algorithm still requires quite a large domain [see $\delta\Omega_{\text{inj}}$ in Fig. 1(b)] to properly define the initial state.

Many of the above strategies available in the literature have been developed for the one-dimensional (1D) case with no easy implementation to higher dimensionality. Some exceptions for two-dimensional (2D) extensions involving time convolution integrals with a near-optimal complexity can be found in Refs. [29,30]. To apply absorbing boundary conditions in a realistic electronic device simulator [16,20,21], one is interested in an algorithm (i) with a negligible increment of the computational effort, (ii) that is easily generalizable to 2D and 2D quantum systems, and (iii) that is not restricted to the continuous Schrödinger equation but is also applicable to atomistic tight-binding equations (which are nowadays quite common in quantum transport where transport and band-structure phenomena are fully mixed). Among the above methods, the one based on the attenuation layer [24,31] schematically represented in Fig. 1(b) fulfills these requirements. However, to the best of our knowledge, in the attenuation layer method (in fact, in all previous works on absorbing boundary conditions for the time-dependent wave function [23–33]), the simulation domain is selected so that the support of the initial state perfectly fits inside the domain, i.e., there is an injection layer large enough to contain the whole initial state when applied to transport. See $\delta\Omega_{\text{inj}}$ in Fig. 1(b). Although this condition seems reasonable, we will see in this work that it implies an important computational drawback for time-dependent quantum transport. Indeed, a general scenario for modeling quantum transport assumes a time-dependent inhomogeneous potential in the active region Ω' and a homogeneous potential outside. The initial wave function is located outside Ω' in $\delta\Omega_{\text{inj}}$ [see Fig. 1(b)]. For example, a typical scenario is a (tunneling) barrier of a few nanometers plus an initial wave function located far from the barrier (i.e., outside Ω') and whose spatial dispersion is tens of nanometers (even much larger than the active region itself). The evolution of the initial wave function before impinging with the barrier is quite trivial. Under these circumstances, we demonstrate in Sec. III A that it is possible to avoid the injection layer $\delta\Omega_{\text{inj}}$ and reduce the domain to $\delta\Omega'_{\text{out}} \cup \Omega' \cup \delta\Omega'_{\text{out}}$ as depicted in Fig. 1(c) using a simple and general injection algorithm. Moreover, in Sec. III B we also present a variant to the absorbing boundaries employing attenuation layers similar to [31] but exploiting a change of coordinates (which we call remapping; see Sec. III C) of the attenuation layer that allows a sensible reduction of the width of attenuation layer itself [$\delta\Omega'_{\text{out}} \ll \delta\Omega_{\text{out}}$; Fig. 1(c)] as proved in Sec. IV. These simulation schemes imply an unprecedented reduction of the computational burden associated with numerical simulations of time-dependent wave packets. Finally, even if in this work we present the 1D case only for the sake of compactness and clarity, the generalization to two and three dimensions is possible even if not completely trivial due to some issues arising in higher dimensions not fully treated here (errors depend in a complicated way on the angle of incidence). However, this work represents the seed for future generalization to higher dimensions.

II. GENERAL CONSIDERATION

We study the time-dependent transport of particles (electrons) in a tunneling region. Below, we present a brief summary

of the effective mass and tight-binding formulation of the Schrödinger equation relevant for this work.

A. The Hamiltonian

We consider the time-dependent Schrödinger equation:

$$i\hbar\frac{\partial|\psi(t)\rangle}{\partial t} = (\hat{H}_0 + \hat{U})|\psi(t)\rangle, \tag{1}$$

where $|\psi(t)\rangle$ is a state and $\hat{H} = \hat{H}_0 + \hat{U}$ is the Hamiltonian in some particular Hilbert space that splits into the free-particle Hamiltonian $\hat{H}_0$ (i.e., no interactions are included), and the potential operator $\hat{U}$ that represents interaction with external force fields. First, given the position state $|x\rangle$, we can define the wave function $\psi(x,t) = \langle x|\psi(t)\rangle$ and its (effective mass) Hamiltonian as follows:

$$\langle x|\hat{H}_{\rm em}|\psi(t)\rangle = -\frac{\hbar^2}{2m^*}\frac{\partial^2\psi(x,t)}{\partial x^2} + U(x,t)\psi(x,t), \tag{2}$$

where m^* is the particle (effective) mass and $U(x,t)$ is the external potential. Second, since the work is motivated for electronic transport (in crystal materials), we discuss also a particle in the Hilbert space defined by the (1D regularly distributed) M atom positions, $x_j = j\Delta x$ being Δx the distance between atoms. The state of the system is defined now as $\psi_j(t) = \langle j|\psi(t)\rangle$ and the (1D nearest-neighbor tight-binding) Hamiltonian

$$\hat{H}_{tb} = \sum_{j=1}^{M} \rho|j\rangle\langle j| + u|j\rangle\langle j+1| + u|j\rangle\langle j-1| + U_j(t)|j\rangle\langle j|, \tag{3}$$

where $U_j(t) = U(x_j,t)$ and $|j\rangle$ are the (Wannier) states associated with the j atom. We assume that all $|j\rangle$ form a complete $\sum_{j=1}^{M}|j\rangle\langle j| = \mathbf{1}$ and orthonormal $\langle i|j\rangle = \delta_{ij}$ set. It is very enlightening to rewrite (3) in the j-site representation:

$$\langle j|\hat{H}_{\rm tb}|\psi\rangle = u(\psi_{j-1} + \psi_{j+1}) + \rho\psi_j + U_j\psi_j, \tag{4}$$

where (for compactness) we have not written the time dependence of the state. The generalization of (2) and (4) to 2D and 3D cases is straightforward, and it will be discussed briefly in the Conclusions section.

B. Hamiltonian eigenstates and eigenvalues

Let us consider the free-particle Hamiltonian $\hat{H}_0$. Then, in the effective-mass scenario, the Hamiltonian eigenfunctions are plane waves $|k\rangle_{\rm em} = 1/\sqrt{2\pi}\int\exp(ikx)|x\rangle dx$ with eigenvalues

$$E_{\rm em}(k) = \frac{\hbar^2k^2}{2m^*} \tag{5}$$

for any value of the wave vector k.

On the other hand, the tight-binding $\hat{H}_0$ has eigenkets $|k\rangle_{\rm tb}$ of the form of Bloch eigenfunctions:

$$|k\rangle_{\rm tb} = \sum_{j=1}^{M} e^{ikj\Delta x}|j\rangle \tag{6}$$

for $k \in [-\pi/\Delta x, \pi/\Delta x]$, with eigenvalues

$$E_{\rm tb}(k) = \rho + 2u\,\cos(k\Delta x), \tag{7}$$

which represent the so called (E-k) dispersion relationship.

C. Localized initial state in a flat potential region

As mentioned in Fig. 1, the entire quantum domain is *artificially* divided into two reservoirs (left and right) plus an interaction box Ω'. At the initial time, the wave function of the particle (electron) is fully localized in one of the reservoirs, while at a final time, its probability presence is delocalized into the left or right reservoirs (but not in Ω'). The initial state can be written as a proper superposition of a Hamiltonian eigenstate, whose time evolution (inside the reservoir) can be written, in general [34], as

$$|\psi(t)\rangle = \int_{-\infty}^{\infty} a(k)e^{-iE(k)(t-t_0)/\hbar}|k\rangle dk \tag{8}$$

with $a(k) = \langle k|\psi(t_0)\rangle$. For (2), a very reasonable assumption for computing (8) analytically in a flat-potential reservoir is the following Gaussian wave packet:

$$\psi_G(x,t) = \left[\frac{\sigma_0^2}{2\pi\left[\sigma_0^4 + \sigma_x^4(t)\right]}\right]^{\frac{1}{4}} e^{i[\varphi(t)+k_x(x-x_0)]} \times \exp\left[-\frac{[x - x_0 - 2k_x\sigma_x^2(t)]^2}{4\left[\sigma_0^2 + i\sigma_x^2(t)\right]}\right], \tag{9}$$

where σ_0 is the spatial variance of the wave packet at $t = 0$, x_0 the initial central position, $\sigma_x^2(t) = \hbar t/2m^*$, k_x the central wave vector, and $\varphi(t) = -\theta(t) - k_x^2\hbar t/2m^*$, with $\theta(t)$ the solution of $\sigma_0^2\tan(2\theta) = \hbar t/2m^*$. Moreover, it can be simply verified that $\int_{-\infty}^{\infty}|\psi_G(x,t)|^2dx = 1$

Equivalently, the same Gaussian wave function can be used as the initial state for the tight-binding model with

$$\psi_{G_i}(0) = \langle i|\psi_G(0)\rangle = \psi_G(x_i,0)/N, \tag{10}$$

where N is a constant for a proper normalization. Strictly speaking, $\psi_{G_i}(0)$ is not a spatial wave function but a spatial envelope wave function.

III. METAMATHEMATICAL ALGORITHMS

After interacting in Ω', the wave function freely spread out in the domain Ω of Fig. 1(a). Our model to shorten the simulation box is based on analytical injection, plus absorbing and remapping algorithms. We will see that the simultaneous use of all these techniques provides the shortest simulation box, with a negligible error and a very small additional computational effort.

A. Analytical injection

Since we are interested in time-dependent wave packets whose initial states are localized in the left (or right) reservoir, it would seem that one would have to include the layer $\delta\Omega_{\rm inj}$ in Fig. 1(b) as an avoidable part of the simulation box. As we discuss in Sec. II C, the time evolution of a wave function in the $\delta\Omega_{\rm inj}$ is quite predictable, and even analytical for some initial states, such as, for example, Gaussian wave packets [see Eq. (9)]. Therefore, one can envision an algorithm to avoid the

explicit consideration of the reservoirs in the simulation box (during the injection process). To pursue this goal, we present an injection algorithm that can work for both the effective-mass and tight-binding Hamiltonians discussed in this work.

1. State split

The state $|\psi\rangle$ solution of Eq. (1) in the whole domain Ω can be decomposed as

$$|\psi(t)\rangle = |\psi_0(t)\rangle + |\phi(t)\rangle, \tag{11}$$

where $|\psi_0\rangle$ is the free-particle solution [i.e., the solution of Eq. (1) with $\hat{U} = 0$]. Using the linearity of the Schrödinger equation, it can be found that $|\phi(t)\rangle$ is a solution of

$$i\hbar\frac{\partial|\phi(t)\rangle}{\partial t} = (\hat{H}_0 + \hat{U})|\phi(t)\rangle + \hat{U}|\psi_0(t)\rangle, \tag{12}$$

where $\hat{U}|\psi_0(t)\rangle$ is a source term (relevant when the potential is different from zero). By construction, we have the initial condition $|\phi(0)\rangle = 0$.

The decomposition (11) can be very useful to simulate injection of particles into Ω' if we are able to analytically determine $\langle x|\psi_0\rangle$ because we would not need to calculate it outside Ω'. In fact, $\langle x|\phi\rangle$ starts to become different from 0 only when a non-negligible part of $\langle x|\psi_0\rangle$ interacts with the potential, i.e., when $\langle x|\psi_0\rangle$ arrives inside Ω'. By means of absorbing layers $\delta\Omega_{\text{out}}$, we can cancel out the part of $\langle x|\phi\rangle$ that starts to flow out of Ω'. Thus, the aim of the next section is to derive a unified analytical $\langle x|\psi_0\rangle$ that works with both effective mass and tight-binding Hamiltonians.

2. Unified Gaussian free-particle evolution

From the literature, we only know the analytical $\psi_0(x,t) = \langle x|\psi_0(t)\rangle$ solution of an effective-mass Hamiltonian for a free particle in flat potentials; see Eq. (9). For the 1D atomistic tight-binding Hamiltonian, we do not have an analytical solution for a free-particle Hamiltonian, however we can derive an approximate analytical solution that works accurately within many simulation cases of interest.

We consider the initial state for $\langle x|\psi_0(t)\rangle$ given by (10), and from Eq. (4), assuming $\hat{U} = 0$ and omitting for simplicity the subscript 0 of ψ_0 and the dependence on t, we have

$$\langle j|\hat{H}_0|\psi\rangle = u(\psi_{j-1} - 2\psi_j + \psi_{j+1}) + (\rho + 2u)\psi_j, \tag{13}$$

where, from Sec. II A, $\psi_j = \langle j|\psi\rangle = \psi(x_j)$ and $\psi_{j\pm1} = \langle j \pm 1|\psi\rangle = \psi(x_j \pm \Delta x)$. Thus, using the Taylor series $\psi_{j+1} = \sum_{r=0}^{\infty}\frac{1}{r!}\frac{\partial^r}{\partial x^r}\psi_j\Delta x^r$ [where $\frac{\partial^r}{\partial x^r}\psi_j = \frac{\partial^r}{\partial x^r}\psi(x)|_{x=x_j}$] and similarly for ψ_{j-1} and substituting into (13), we have

$$\psi_{j+1} - 2\psi_j + \psi_{j-1} = 2\sum_{r=1}^{\infty}\frac{1}{(2r)!}\frac{\partial^{2r}\psi_j}{\partial x^{2r}}\Delta x^{2r}. \tag{14}$$

Now, looking at (9) the initial state is a product of two exponentials, however the first exponential contains the stronger spatial variation of ψ_0, so we can neglect the spatial derivative of the second exponential to obtain

$$\frac{\partial^{2r}\psi_G(x)}{\partial x^{2r}} \approx (ik_x)^{2(r-1)}\frac{\partial^2\psi_G(x)}{\partial x^2}. \tag{15}$$

In addition, since we have assumed that the initial state for $\langle x|\psi_0(t)\rangle$ is given by (10), we can substitute (15) into (14) to obtain

$$\psi_{G_{j+1}} - 2\psi_{G_j} + \psi_{G_{j-1}} \approx -\frac{2}{k_x^2}\frac{\partial^2\psi_{G_j}}{\partial x^2}\sum_{r=1}^{\infty}\frac{(ik_x\Delta x)^{2r}}{(2r)!}, \tag{16}$$

and using the Taylor series of the cosine on the right-hand side of (16), we have

$$\psi_{G_{j+1}} - 2\psi_{G_j} + \psi_{G_{j-1}} \approx 2\frac{1-\cos(k_x\Delta x)}{k_x^2}\frac{\partial^2\psi_{G_j}}{\partial x^2}. \tag{17}$$

Finally, substituting (17) into (13) and defining the new time

$$t'(t) = -\frac{4um^*[1-\cos(k_x\Delta x)]}{\hbar^2k_x^2}t, \tag{18}$$

it is simple to prove that the function

$$\psi_{\text{an}}(x,t) = e^{-it(\rho+2u)/\hbar}\psi_G(x,t'(t)), \tag{19}$$

under the above approximations, satisfies the tight-binding version of Eq. (1) for $\hat{U} = 0$.

We can easily prove that the analytical solution (19) is not only a unified solution for both the effective-mass and tight-binding free-particle of Eq. (1) with initial condition $\psi_G(x,0)$, but it is also valid for the discretized version of the effective-mass Hamiltonian commonly used in numerical simulations,

$$\langle j|\hat{H}_0|\psi\rangle = -\frac{\hbar^2}{2m^*}\frac{\psi_{j+1} - 2\psi_j + \psi_{j-1}}{\Delta x^2}. \tag{20}$$

In fact, (20) corresponds to (13) when we consider $\rho = -2u$ and $u = -\hbar^2/(2m^*\Delta x^2)$. Moreover, if we further consider small k_x, we have $t' \approx t$ and $E_{\text{tb}}(k) = \hbar^2k^2/(2m^*) = E_{\text{em}}(k)$, meaning that the tight-binding model coincides with the effective-mass theory only close to the bottom of the conduction band.

In Fig. 2, the solution (19) is compared with the numerical solution for $\rho = -2u$ and $u = -\hbar^2/(2m^*\Delta x^2)$ at different values of k_x obtained by inverting the relation $E(k_x) = \hbar^2k_x^2/(2m^*)$. It can be seen that it leads to excellent agreement between the numerical solution and the analytical one even for high energies.

B. Absorption

The injection algorithm avoids the simulation of the quantum state outside Ω' before and in a short time after the interaction occurring within Ω'. However, after a long enough time (but much shorter than the typical simulation time), the quantum state $\langle x|\phi\rangle$ defined in Sec. III A 1 starts to spread out, Ω'. Thus, in order to avoid the simulation out of Ω', we are interested in a function $\Psi(x,t)$ that would be equal to the solution $\psi(x,t)$ of Eq. (1) in Ω', i.e., $\Psi(x,t) = \psi(x,t)$ at $x \in \Omega'$, but that could vanish outside, i.e., $\Psi(x,t) \approx 0$ for $x \notin \Omega'$. To achieve this goal, we discuss a modified version of a well-known absorbing algorithm [31].

Let us consider Ω' defined by $a \leqslant x \leqslant b$ with $a < b$ and $a,b \in \mathbb{R}$. For $x \geqslant b$ and $x \leqslant a$, the potential U is assumed to be uniform. With no loss of generality, we take $b = 0$ and we discuss the boundary condition for $x \geqslant b$ only. We define the

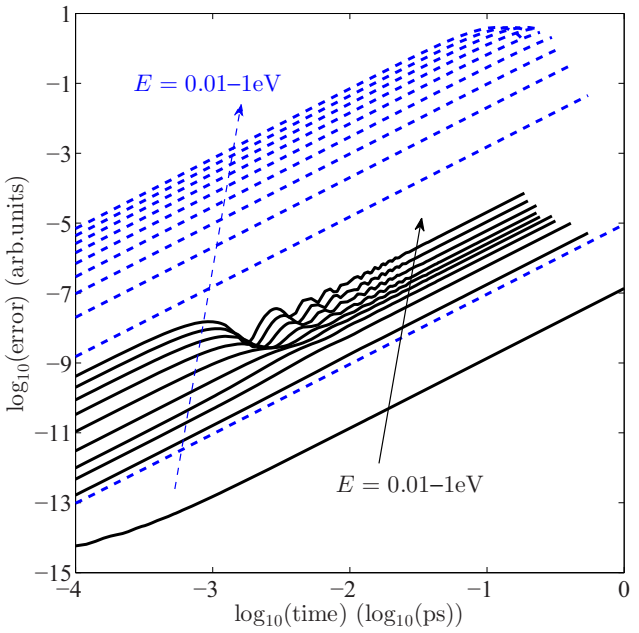

FIG. 2. (Color online) Simulation of a Gaussian wave packet of a free particle with $E = \hbar^2 k_x^2/(2m^*) = 0.01$–1 eV equally spaced into 10 values, $\sigma_0 = 25/\sqrt{2}$ nm, and initially centered in $x_0 = -70$ nm and $m^* = 0.2m_0$, where m_0 is the free-electron mass. The simulation parameters are $\Delta t = 0.01$ fs, $\Delta x = 0.2$ nm, the full simulation space ranges from -800 to 800 nm, and the simulation is stopped when $\int_{-800\text{ nm}}^{50\text{ nm}} |\psi_0|^2 dx < 10^{-10}$. The dashed blue line is $\log[\|\psi_{G_{\text{num}}}(t) - \psi_G(t)\|^2]$, and the solid black line is $\log(\|\psi_{G_{\text{num}}}(t) - \psi_{\text{an}}(t)\|^2)$, where $\psi_{G_{\text{num}}}$ is the numerical solution for the Gaussian free particle, ψ_G is the analytical solution (9), and ψ_{an} is the analytical solution given by (19).

function f as

$$f(x) = \begin{cases} g(x) & \text{for } x > 0, \\ 1 & \text{for } x \leqslant 0, \end{cases} \tag{21}$$

with $g(x)$ a real positive smooth function smaller than 1. The goal is to define a recursive algorithm to make ψ vanish in a region $0 < x \leqslant L$ (the absorbing layer $\delta\Omega_{\text{out}}$) for some $L > 0$ without perturbing the part of the wave function belonging to Ω'. Using the central difference scheme to integrate (1), the first iteration reads

$$\psi^2 = \psi^0 + \frac{\Delta t}{i\hbar}\hat{H}\psi^1, \tag{22}$$

where $\hat{H}$ is the Hamiltonian $\hat{H} = -\frac{\hbar^2}{2m}\frac{\partial^2}{\partial x^2} + U$ and $\psi^j = \psi(x,t_j)$. Let $\Psi^0 = f\psi^0$ and $\Psi^1 = f\psi^1$, and we modify the first iteration as

$$\Psi^2 = \Psi^0 + \frac{\Delta t}{i\hbar}\hat{H}\Psi^1 = f\psi^0 + \frac{\Delta t}{i\hbar}\hat{H}f\psi^1. \tag{23}$$

Now, we further assume that $f(x)$ is sufficiently smooth to commute with $\hat{H}$, $[f,\hat{H}] \approx 0$, obtaining

$$\Psi^2 = f\left(\psi^0 + \frac{\Delta t}{i\hbar}\hat{H}\psi^1\right). \tag{24}$$

Iterating the scheme and using (21), we have

$$\Psi^n = f^{n-1}\psi^n = \begin{cases} g(x)^{n-1}\psi(x,t_n) & \text{for } x > 0, \\ \psi(x,t_n) & \text{for } x \leqslant 0. \end{cases} \tag{25}$$

Unfortunately, the function $g(x)$ rigorously satisfying all the previous prescriptions does not exist. Indeed, the unique real function that commutes with $\hat{H}$ and satisfies all the analytical properties stated above is $g(x) = 1$, but it does not satisfy $g(x) < 1$. However, we can require a function that only approximately commutes with $\hat{H}$. This weaker condition can be reached requiring that both the first and second spatial derivatives of $g(x)$ are small enough compared to the spatial derivatives of ψ, at the positions where ψ is not negligible. Among many other possibilities, we can use a slightly decreasing polynomial of the form

$$g(x) = 1 - \left(\frac{x}{L}\right)^m \tag{26}$$

with $m \geqslant 3$. The polynomial (26) for $0 \leqslant x \ll L$ has very small derivatives, so that it commutes approximately with $\hat{H}$, as required. When x approaches L, the derivatives of $g(x)$ increase. However, as shown in Fig. 3, the wave function is absorbed much before $x = L$. Finally, from Fig. 3 it can be seen that the wave function is not perturbed inside Ω', as required.

From Eq. (26), it follows that the boundary condition can be modulated by varying both L and m. To automatically estimate L, we observe that for a Gaussian wave packet, the characteristic length is the de Broglie length $\lambda = 2\pi/k_x$. It is simple to see that if $L \gg \lambda$, then $f(x)$ approximately commutes with $\hat{H}$. One can use this argument to define L. Other criteria for fixing L that satisfy a predetermined error are also possible. In any case, one expects that wave functions

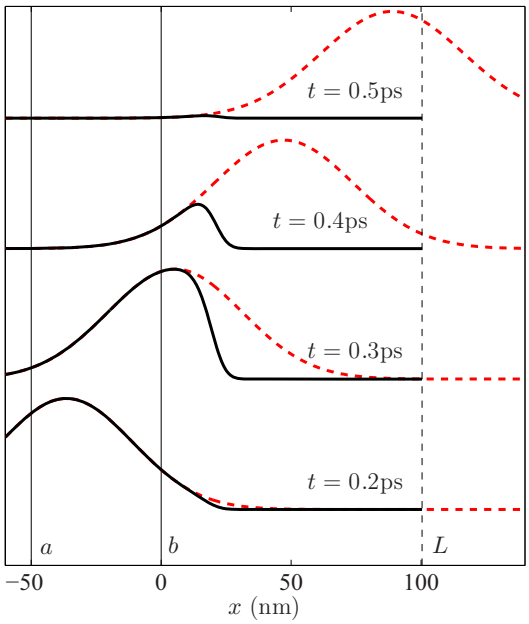

FIG. 3. (Color online) Simulation of a Gaussian wave packet with energy $E = 0.1$ eV, and the other parameters as in Fig. 2. The solid black line is the absorbed wave packet with $L = 100$ nm, and the dashed red line is the wave packet given by (9).

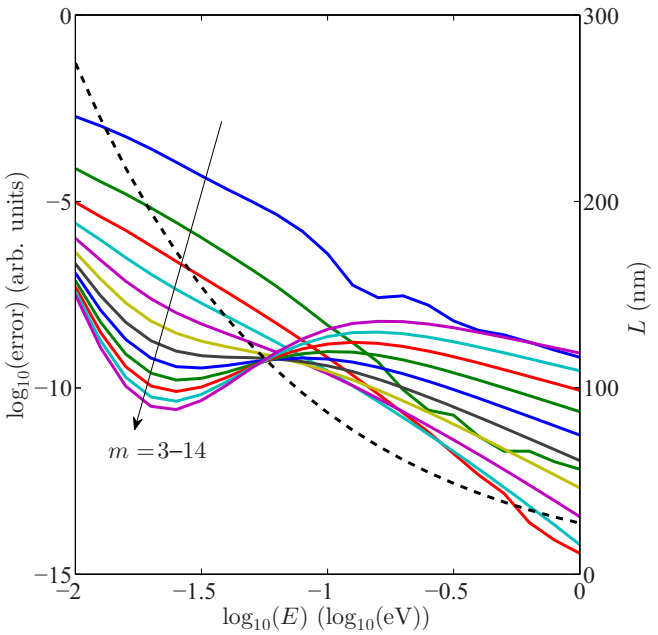

FIG. 4. (Color online) Simulation of a Gaussian wave packet of a free particle with the same parameters as in Fig. 2. The simulation parameters are as follows: the full simulation space ranges from −800 to 800 nm, $a = -800$ nm, $b = 50$ nm, and the length L, taken as 10λ, is the dashed black line referring to the right y axis. The solid lines are $\log_{10}(\varepsilon_{\text{abs}})$.

with high energies require a smaller L than that of low-energy wave functions. It is worth noting that for zero applied bias, if in Ω' the wave packet interacts with some potential barrier, the transmitted and reflected waves have momenta that are in general close to the initial one (apart from a sign), so the length L can be simply related to the initial de Broglie length. When a bias is applied, there is an asymmetry between the right and left wavelengths of the wave packet that needs to be taken into account.

We have carried out simulations to determine the impact of m on the error of the absorbing argument. In Fig. 4, we evaluated the error function $\varepsilon_{\text{abs}} = \max_{t\in\mathbb{R}_+}[\int_a^b |\psi_{G_{\text{num}}}(t) - \Psi_{G_{\text{abs}}}(t)|^2 dx]$, where $\psi_{G_{\text{num}}}$ is the numerical solution of the Schrödinger equation calculated in the full spatial domain, i.e., the domain Ω in Fig. 1(a), and $\Psi_{G_{\text{abs}}}$ is the solution obtained for the wave function absorbed with L depending on the initial energy of the wave packet. Thus, looking at Fig. 4, the best compromise for m, i.e., the best behavior for high and low energies, is $5 \leqslant m \leqslant 7$.

We finally mention that this absorbing algorithm is equivalent to introducing in Eq. (1) a negative imaginary potential nonvanishing outside Ω', as discussed in Appendix.

C. Remapping

As mentioned above in the results of Fig. 4, wave functions with small energies require large absorbing layers, $\delta\Omega_{\text{out}}$. For such small energies, one can expect a reduction of the error, without increasing the number of grid points, by a proper remapping of the absorbing layers. Let us consider the same simulation domain of the preceding section with Ω' defined by $a \leqslant x \leqslant 0$. For $x \geqslant 0$, we define the variable change

$$z = c(x) = K \arctan \frac{x}{K}. \tag{27}$$

This maps x into z with a consequent contraction of the spatial domain, in fact for $x \in [0, +\infty]$ we have $z \in [0, K\pi/2]$. Moreover, deriving (27), we have $dz/dx = K^2/(K^2 + x^2)$, that in $x = 0$ is equal to 1, meaning that the contraction map is smooth in the whole spatial domain. We can unambiguously define the inverse map for $z \in [0, K\pi/2]$ as

$$x = c^{-1}(z) = K \tan \frac{z}{K}. \tag{28}$$

Using (27) and (28), we can rewrite the Schrödinger equation (1) for $x \in [0, +\infty]$ with wave function $\psi(c^{-1}(z), t)$ using the transformed Hamiltonian

$$\hat{H}_z = -\frac{\hbar^2}{2m^*}\left[c'[c^{-1}(z)]^2 \frac{\partial^2}{\partial z^2} + c''[c^{-1}(z)]\frac{\partial}{\partial z}\right] + U(c^{-1}(z), t), \tag{29}$$

where $c'(x) = dc(x)/dx = K^2/(K^2 + x^2)$ and $c''(x) = d^2c(x)/dx^2 = -2K^2x/(K^2 + x^2)^2$. Using (28), these expressions give $c'[c^{-1}(z)]^2 = \cos^4(z/K)$ and $c''[c^{-1}(z)] = -2/K \sin(z/K)\cos^3(z/K)$.

Let us define L_a as the width of the spatial domain outside Ω', so the spatial domain is divided into $a - L_a \leqslant z < a$ (left augmented boundary), $a \leqslant x \leqslant b$ (Ω'), and $b < z \leqslant b + L_a$ (right augmented boundary). Thus, the remapping parameter K of (27) is assumed to be equal for both sides because the augmented boundaries are the same. It is worth noting that, for a correct implementation, we take $K = 2L_a/\pi$, implying $c^{-1}(a - L_a) = -\infty$ and $c^{-1}(b + L_a) = \infty$. To discuss the numerical results when we implement the remapping algorithm, we assume $a = -\infty$, so no injection is needed. We define $\varepsilon_{\text{rem}} = \int_a^b |\psi_{\text{full}} - \psi_{\text{rem}}|^2 dx$, where ψ_{full} is the numerical solution of the free particle in an infinite (large enough) domain and ψ_{rem} is the numerical solution using the remapping on the right side of the domain. Moreover, we define $\varepsilon_{\text{cut}} = \int_a^b |\psi_{\text{full}} - \psi_{\text{cut}}|^2 dx$, where ψ_{cut} is the numerical solution in the domain $-\infty < x \leqslant b + L_a$. From Fig. 5, it is worth noting that, when we implement the remapping, after a certain delay the error ε_{rem} starts growing. This is due to the fact that when we numerically implement the Hamiltonian (29), the differential part corresponds to a discretized second derivative in x with a Δx growing as $\Delta x = K \tan(\Delta z/K)$ [we used Eq. (28)]. Because of the considerations in Sec. III A 2, a slowdown of the wave function occurs. However, when $K \tan(\Delta z/K)$ grows too much, the wave function is reflected and it returns to Ω'. So basically we have the same behavior of a wave function simulated in the domain $-\infty < x \leqslant b + L_a$ (see the error ε_{cut} in Fig. 5) with the unique difference that the reflection is retarded.

IV. PRACTICAL IMPLEMENTATION

Starting from the considerations in the previous sections, we can devise an algorithm that can overcome all the drawbacks reported above. The idea is to combine all the previous algorithms in such a way that they compensate for their drawbacks. The simultaneous employment of those algorithms

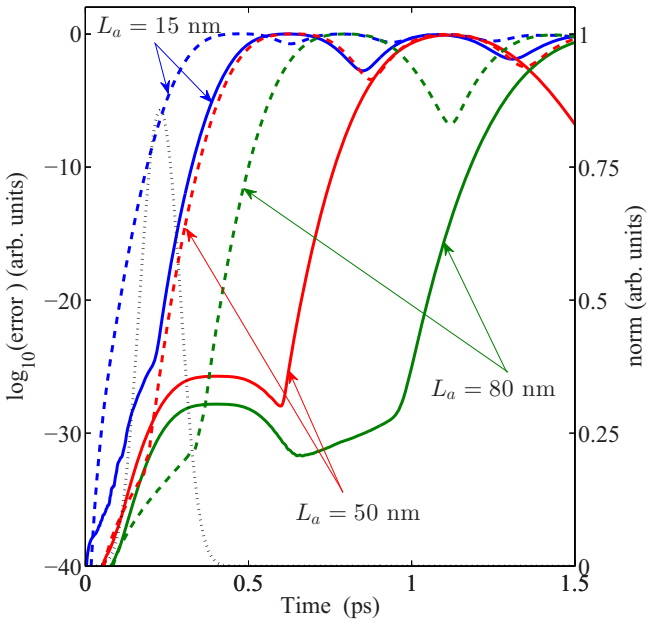

FIG. 5. (Color online) Simulation of a Gaussian wave packet of a free particle with the same parameters as in Fig. 2. The simulation parameters are as follows: $E = 0.1$ eV, the full simulation space ranges from -800 to 800 nm, $a = -800$ nm, and $b = 50$ nm. The dotted black line referring to the right y axis is the norm $\int_{-800\text{ nm}}^{50\text{ nm}} |\psi_G|^2 dx$. The solid lines are $\log_{10}(\varepsilon_{\text{rem}})$ and the dashed lines are $\log_{10}(\varepsilon_{\text{cut}})$.

TABLE I. Pseudocode for simultaneous implementation of injection, absorption, and remapping algorithms. Product .* denotes element-by-element multiplication between vectors.

```
%Main definitions
ib = a≤x≤b                          %Points inside Ω'
il = x<a, ir = x>b                  %Points outside Ω'
K = 2*La/pi                         %Remapping parameter
L = 10*(2*pi/kx)                    %Absorption parameter
tc = 2*(1-cos(kx*dx))/(kx*dx)^2     %Time correction
                                    constant
zl = a+K*tan((x(il)-a)/K)           %Variable change
zr = b+K*tan((x(ir)-b)/K)           %Variable change
g(il) = 1-(a-zl)^n*L^-n             % f(x) for x < a
g(ir) = 1-(zr-b)^n*L^-n             % f(x) for x > b
%Cycle over time steps
do j = 1..N
                %Solve for φ
   phi2(il) = g(il).*(phi0(il)+Hzl*phi1(il)+
                U(zl,t_j).*(phi1(il)+psi1_0(il)))
   phi2(ib) = phi0(ib)+H*phi1(ib)+
                U(ib,t_j).*(phi1(ib)+psi1_0(ib))
   phi2(ir) = g(ir).*(phi0(ir)+Hzr*phi1(ir)+
                U(zr,t_j).*(phi1(ir)+psi1_0(ir)))
   phi0 = phi1, phi1 = phi2
                %Solve for ψ0
   psi2_0(il) = psi0_an(zl,t_j*tc)
   psi2_0(ib) = psi0_0(ib)+H*psi1_0(ib)
   psi2_0(ir) = g(ir).*(psi0_0(ir)+Hzr*psi1_0(ir)
   psi0_0 = psi1_0, psi1_0 = psi2_0

end do
```

is aimed at simulating the Schrödinger equation, using as spatial support Ω' plus small absorbing layers $\delta\Omega'_{\text{out}}$. In Table I, a pseudocode for simultaneous implementation is presented. We discuss here the main idea and some implementation details to improve the accuracy of the simulation.

Let L and L_a be as in Secs. III B and III C, respectively. We further define an effective augmented length $L_{\text{eff}} \leqslant L_a$ such that $L_{\text{eff}} = K \arctan L/(2K)$, and this is the width of the absorbing layer, $\delta\Omega'_{\text{out}}$. So, in this picture, the spatial domain is now divided into $a - L_{\text{eff}} \leqslant z < a$ ($\delta\Omega'_{\text{out}}$ on the left), $a \leqslant x \leqslant b$ (Ω'), and $b < z \leqslant b + L_{\text{eff}}$ ($\delta\Omega'_{\text{out}}$ on the right). Thus, L_a is, in this case, the maximum augmented boundary when $L = \infty$. The remapping parameter K is still evaluated through L_a as in Sec. III C. The absorbing parameter L has to be chosen sufficiently larger than the de Broglie length to guarantee $L \gg \lambda$. Here we take $L = 10\lambda$. It is worth noting that the function $g(x)$ has been consistently evaluated with the remapping to guarantee the efficiency of the absorption algorithm, i.e., Eq. (26) must be remapped through (28) (see Table I).

In this picture, we assume for simplicity that the particle is injected from the left reservoir (injection from the right follows straightforwardly). We use the injection algorithm discussed in Sec. III A. In Table I, the evaluation of ψ_0 is analytical only in part. In fact, assuming that the packet comes from the left reservoir, it is analytically evaluated only there following Eq. (9) and remapped through (28). Even if in the rest of the domain ψ_0 is numerically evaluated, this does not increase the numerical burden because the number of floating point operations is practically the same. On the contrary, this choice permits us to consistently implement the absorption algorithm also for ψ_0, which from numerical tests results in a more accurate solution.

The remapping and absorbing algorithms are used simultaneously in the absorbing layers. The first has as a practical effect the slowdown of the wave function inside the absorbing layers, while the absorbing algorithm cuts down the wave function avoiding the reflection discussed in Sec. III B. This allows us to use very small absorbing layers to simulate the wave function. To give a practical example, in Fig. 6 we reported the simulation of a particle interacting with a potential barrier for three different energies $E = 0.01$, 0.1, and 1 eV. The direct implementation of the absorbing algorithm would require the absorbing layers $\delta\Omega_{\text{out}}$ large, at least $L/2 = 137$, 43.4, and 13.7 nm, respectively (see Sec. III B). On the contrary, using the remapping algorithm, we can take $L_a = 20$ nm, and as consequence the with of $\delta\Omega'_{\text{out}}$ is $L_{\text{eff}} = 18.9$, 16.4, and 10.5 nm, resulting in much smaller absorbing layers, especially for small energies.

When we solve for ϕ and ψ_0 (where the solution is not analytical) in Table I, we use a central difference scheme for the time derivative that is an explicit method, stable for the Schrödinger equation, widely used, and discussed exhaustively in [35]. However, the choice is not mandatory and the entire algorithm can be simply modified according to other finite-difference schemes for the time derivative. The Hamiltonians H and H_z can be evaluated using normal finite-difference

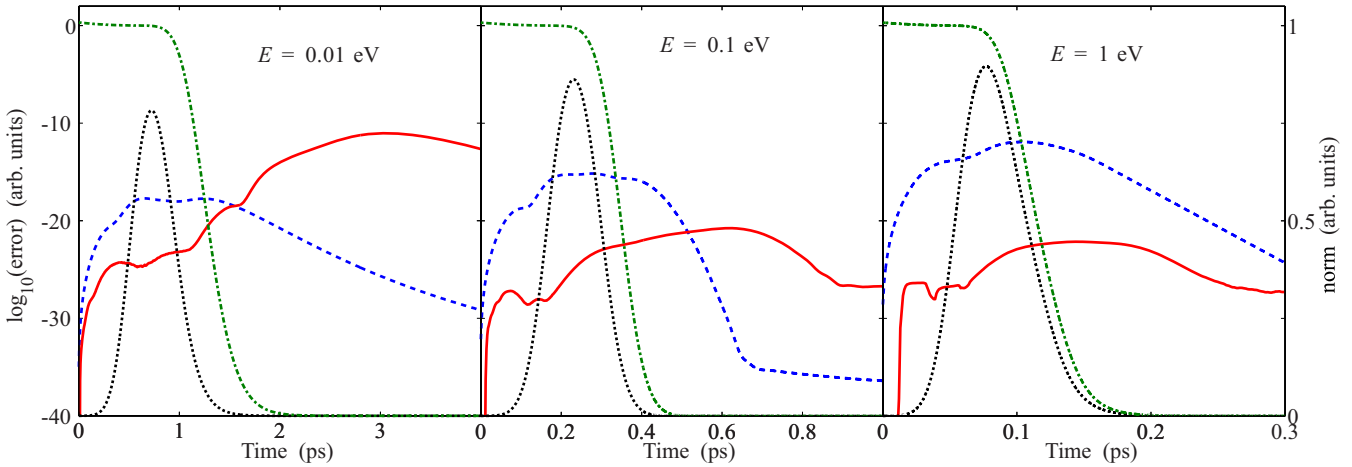

FIG. 6. (Color online) Simulation of a Gaussian wave packet with the same parameters as in Fig. 2. The simulation is carried out for the three energies $E = 0.01$, 0.1, and 1 eV, and the wave packet interacts with a potential barrier centered at 27.5 nm with a width of 5 nm and heights of 0.015, 0.0825, and 0.93 eV, respectively. The different barrier heights guarantee that the transmitted and reflected waves after interaction have the same norm for each energy, guaranteeing that the absorbing and remapping algorithms work equally well on both sides of Ω'. The full simulation space ranges from -800 to 800 nm, Ω' from $a = 0$ nm to $b = 50$ nm, the absorbing layers have $L_a = 20$ nm, $L = 274$, 86.8, and 27.4 nm (corresponding to double the width of $\delta\Omega_{\text{out}}$), and $L_{\text{eff}} = 18.9$, 16.4, and 10.5 nm (corresponding to the width of $\delta\Omega'_{\text{out}}$), respectively, depending on the initial wave-packet energy, and finally the absorption exponent is $m = 5$. The dashed blue line is $\log(\varepsilon_{\text{inj}})$ and the solid red line is $\log(\varepsilon_{\text{ar}})$, and they refer to the left y axis. The dotted black line is the evolution of the norm $\int_a^b |\psi_{\text{num}}|^2 dx$ and the dashed-dotted green line is the evolution of the norm $\int_{a-L_a}^{a} c^{-1}(z)|\Psi_{\text{new}}|^2 dz + \int_a^b |\Psi_{\text{new}}|^2 dx + \int_b^{b+L_a} c^{-1}(z)|\Psi_{\text{new}}|^2 dz$, and it refers to the right y axis.

schemes. In Table I, H, H_z, and U are implicitly multiplied by $2\Delta t/(i\hbar)$.

Finally, in Fig. 6 the error of the method is reported. We simulated a Gaussian wave packet interacting with a potential barrier. We have defined three different solutions to estimate different sources of errors. The first is ψ_{num}: the full numerical solution obtained using a large enough spatial domain to avoid boundary effects. The second is ψ_{inj}: the solution with a large spatial domain including the injection algorithm implemented as in Table I. The last is Ψ_{new}, the solution in the small domain including all the algorithms implemented as in Table I. Using these different solutions, we define the errors $\varepsilon_{\text{inj}} = \int_a^b |(\psi_{\text{num}} - \psi_{\text{inj}})|^2 dx$ due to the injection algorithm only, and $\varepsilon_{\text{ar}} = \int_a^b |(\psi_{\text{inj}} - \Psi_{\text{new}})|^2 dx$ due to the absorbing and remapping algorithm used simultaneously. As can be seen from the caption of Fig. 6, the small domain $\delta\Omega'_{\text{out}} \cup \Omega' \cup \delta\Omega'_{\text{out}}$ (of width $50 + 2L_{\text{eff}}$ nm) is much smaller than the full domain Ω (1600 nm), by about two orders of magnitude, and than the domain $\delta\Omega_{\text{out}} \cup \delta\Omega_{\text{inj}} \cup \Omega' \cup \delta\Omega_{\text{out}}$ (of width $50 + 200 + 2L/2$), by about one order of magnitude, resulting in an extreme reduction of the computational burden. The error ε_{inj} is always very small (negligible) for any energy. Coupling the absorbing algorithm to the remapping, we contract the entire x domain inside the augmented boundary and consequently the absorbing algorithm can properly work, as ε_{ar} proves. Finally, we observe that the total error of our algorithm follows $\varepsilon_{\text{tot}} \leqslant \varepsilon_{\text{inj}} + \varepsilon_{\text{ar}}$, which in a log scale of Fig. 6 means that it is the maximum between them.

V. CONCLUSIONS

In the literature, most of the efforts to deal with quantum dynamics are still based on the use of Hamiltonian or momentum eigenstates. However, one of these states cannot describe an electron localized at the right or left of the barrier because they extend everywhere at any time [9]. In other words, Hamiltonian or momentum eigenstates (or scattering states) do not belong to the Hilbert space because they cannot be normalized to unity. Additionally, any attempt to include many-body physics in single-particle solutions (for example, with the use of conditional Bohmian wave functions) also requires explicit time-dependent equations. However, the practical solution of such time-dependent equations has very significant computational problems. One of the reasons for the poor development of an explicit time-dependent quantum model for electron transport is the difficulty in developing accurate and fast algorithms for quantum time-dependent equations.

In this paper, we have presented three mathematical algorithms (analytical injection, absorption, and remapping) that allow accurate and fast simulations for the time-dependent one-dimensional Schrödinger equation with a spectacular reduction of the simulation box. We discuss the advantages and disadvantages of the three algorithms presented in this work as follows:

(i) The analytical injection is extremely useful to simulate injection of particles; we only need to calculate ψ_0 inside Ω'. In addition, there is no limitation of the initial position of the wave packet and, as we proved in Sec. III A 2, this injection model can be used for the continuous as well as for the tight-binding version of the Schrödinger equation.

(ii) By applying an absorption boundary to the simulation box, we eliminate the spurious reflection by cutting down the wave function inside the augmented boundary. Moreover, we can shorten the simulation box without losing the accuracy of simulation. But the wave function with low energy requires

a larger simulation box than that of the high-energy wave function, which is shown in Fig. 4.

(iii) The remapping algorithm used alone has the unique effect of slowing down the wave function in the augmented boundary, but it does not avoid the reflection. However, when coupled with the absorbing boundary algorithm of Sec. III B, it compensates for the drawback of the absorbing algorithm, i.e., it enables the absorbing layer width to be greatly reduced even for low energies.

Finally, we created a model by simultaneously combining all three previous algorithms to simulate quantum transport, which worked well for both low- and high-energy wave functions. The spatial domain can be reduced ($50 + 2L_{\text{eff}}$ nm with, for example, $L_{\text{eff}} = 10.5$ nm) to less than 5% of the original domain (1600 nm) while introducing an almost negligible error. Since the memory needed and the number of operations are proportional to the grid points, a similar percentage of reduction of memory and CPU time can be expected. The generalization to 2D (even 3D) systems can be done straightforwardly with the only requirement that the free evolution of the initial wave packet is well known. For example, an analytical solution of a Gaussian wave-packet solution of the Dirac equation is needed to provide tight-binding simulations of 2D graphene [36,37] with a similar strategy as was used in Sec. III A 2.

All the results developed here for quantum transport can also be applied to many other fields that require a time-dependent solution of the Schrödinger equation, and whose initial states are analytically defined far from the interaction region [1]. Additionally, the injection and absorbing algorithms can also be applied only on one side of the system for those computations that require an explicit spatial knowledge of the transmitted wave packet at the other side, far from the interaction region [19].

ACKNOWLEDGMENTS

The authors acknowledge support from the "Ministerio de Ciencia e Innovación" through the Spanish Project TEC2012-31330 and the Grant Agreement No. 604391 of the Flagship initiative "Graphene-Based Revolutions in ICT and Beyond." Z.Z. acknowledges financial support from the China Scholarship Council (CSC).

APPENDIX: NEGATIVE IMAGINARY POTENTIAL

To prove that the absorbing layer algorithm is equivalent to a negative imaginary potential in the absorbing layer, we consider the one-dimensional time-dependent Schrödinger equation (1) and the simulation box artificially divided into two reservoirs (left and right) and Ω' as in Sec. III B. Then, Ω' is defined by $a \leqslant x \leqslant b$, with $a < b$ and $a,b \in \mathbb{R}$. For $x \geqslant b$ and $x \leqslant a$, the potential U is assumed to be uniform, and for the sake of simplicity we take $b = 0$ and discuss the boundary condition for $x \leqslant b$ only.

We consider the functions f and g defined in (21), and at the time $t = 0$ we define $\Psi(x,0) = f(x)\psi(x,0)$, with $\psi(x,0)$ the initial state of (1). As discussed in Sec. III B, at each time step the wave function $\Psi(x,t)$ can be written as $\Psi(x,t) = f(x)\psi(x,t)$ iff $f(x)$ is sufficiently smooth to commute with Hamiltonian $\hat{H}$. Then at a final time t using (25), we have

$$\Psi(x,t) = f(x)^{t/\Delta t}\psi(x,t), \tag{A1}$$

where Δt is the temporal step [from Eq. (25)] and $t/\Delta t = n - 1$. Rewriting Eq. (A1), we obtain

$$\begin{aligned}\Psi(x,t) &= \exp\left[-\frac{1}{\hbar}\left(-\frac{\hbar}{\Delta t}\log[f(x)]\right)t\right]\\ \times\psi(x,t) &= \exp\left[-\frac{J(x)}{\hbar}t\right]\psi(x,t),\end{aligned} \tag{A2}$$

where we define $J(x) = -\frac{\hbar}{\Delta t}\log[f(x)]$. Thus, inverting (A2), we get

$$\psi(x,t) = e^{\frac{J(x)}{\hbar}t}\Psi(x,t), \tag{A3}$$

and inserting (A3) into (1), we have

$$i\hbar\frac{\partial}{\partial t}e^{\frac{J(x)}{\hbar}t}\Psi(x,t) = \hat{H}e^{\frac{J(x)}{\hbar}t}\Psi(x,t). \tag{A4}$$

Since the function f approximately commutes with $\hat{H}$, we also have $[e^{\frac{J(x)}{\hbar}t},\hat{H}] \approx 0$. Using this commutation rule, developing the time derivative, and dividing by $e^{\frac{J(x)}{\hbar}t}$, Eq. (A4) can be rewritten as

$$i\hbar\frac{\partial\Psi(x,t)}{\partial t} = [\hat{H} - iJ(x)]\Psi(x,t), \tag{A5}$$

proving that the absorbing layer algorithm is equivalent to a negative imaginary potential.

[1] R. W. Robinett, Phys. Rep. **392**, 1 (2004).
[2] P. Domokos, P. Horak, and H. Ritsch, Phys. Rev. A **65**, 033832 (2002).
[3] C. Ruiz, L. Plaja, and L. Roso, Phys. Rev. Lett. **94**, 063002 (2005).
[4] C. Bracher, T. Kramer, and J. B. Delos, Phys. Rev. A **73**, 062114 (2006).
[5] A. Picón, A. Benseny, J. Mompart, J. R. Vázquez de Aldana, L. Plaja, G. F. Calvo, and L. Roso, New J. Phys. **12**, 083053 (2010).
[6] J. Wu, B. B. Augstein, and C. Figueira de Morisson Faria, Phys. Rev. A **88**, 063416 (2013).
[7] M. Büttiker, Phys. Rev. Lett. **65**, 2901 (1990).
[8] M. Büttiker, Phys. Rev. B **46**, 12485 (1992).

[9] A Hamiltonian eigenstate has a time-independent probability $|\psi_E(x,t)|^2 = \rho(x)$. Then, the continuity equation $\partial\rho(x)|\partial t + \nabla J = 0$ implies that either the current density is zero, $J = 0$ (such a selection is not valid for quantum transport), or J is uniform everywhere so that its spatial derivative is zero. The latter means that $\psi_E(x,t)$ is a complex function that extended everywhere in the Hilbert space at any time.

[10] E. Runge and E. K. U. Gross, Phys. Rev. Lett. **52**, 997 (1984).

[11] K. Capelle and E. K. U. Gross, Phys. Rev. Lett. **78**, 1872 (1997).

[12] *Fundamentals of Time-Dependent Density Functional Theory*, edited by M. A. L. Marques, N. T. Maitra, F. M. S. Nogueira, E. K. U. Gross, and A. Rubio, Lecture Notes in Physics (Springer, Berlin, 2012), Vol. 837.

[13] S. Kurth, G. Stefanucci, C.-O. Almbladh, A. Rubio, and E. K. U. Gross, Phys. Rev. B **72**, 035308 (2005).

[14] G. Vignale and M. Di Ventra, Phys. Rev. B **79**, 014201 (2009).

[15] C. Y. Yam, X. Zheng, G. H. Chen, Y. Wang, T. Frauenheim, and T. A. Niehaus, Phys. Rev. B **83**, 245448 (2011).

[16] G. Albareda, D. Marian, A. Benali, S. Yaro, N. Zanghì, and X. Oriols, J. Computat. Electron. **12**, 405 (2013).

[17] X. Oriols and D. K. Ferry, J. Computat. Electron. **12**, 317 (2013).

[18] K. K. Das, Phys. Rev. A **84**, 031601 (2011).

[19] C. K. Tobias Kramer and V. Krueckl, Phys. Scr. **82**, 038101 (2010).

[20] X. Oriols, Phys. Rev. Lett. **98**, 066803 (2007).

[21] F. L. Traversa, E. Buccafurri, A. Alarcon, G. Albareda, R. Clerc, F. Calmon, A. Poncet, and X. Oriols, IEEE Trans. Electron Dev. **58**, 2104 (2011).

[22] A. Alarcón, G. Albareda, F. L. Traversa, and X. Oriols, *Applied Bohmian Mechanics: From Nanoscale Systems to Cosmology* (Pan Stanford, Singapore, 2012), pp. 365–424.

[23] X. Antoine, A. Arnold, C. Besse, M. Ehrhardt, and A. Schädle, Commun. Comput. Phys. **4**, 729 (2008).

[24] J. Muga, J. Palao, B. Navarro, and I. Egusquiza, Phys. Rep. **395**, 357 (2004).

[25] G. Hadley, IEEE J. Quantum Electron. **28**, 363 (1992).

[26] D. Yevick, Y. Yayon, and J. Yu, J. Opt. Soc. Am. A **12**, 107 (1995).

[27] V. Baskakov and A. Popov, Wave Motion **14**, 123 (1991).

[28] A. Arnold, M. Ehrhardt, and I. Sofronov, Commun. Math. Sci. **1**, 501 (2003).

[29] C. Lubich and A. Schädle, SIAM J. Sci. Comput. **24**, 161 (2002).

[30] S. Jiang and L. Greengard, Commun. Pure Appl. Math. **61**, 261 (2008).

[31] R. Kosloff and D. Kosloff, J. Computat. Phys. **63**, 363 (1986).

[32] D. Yevick and B. Hermansson, IEEE J. Quantum Electron. **25**, 221 (1989).

[33] C. W. McCurdy, D. A. Horner, and T. N. Rescigno, Phys. Rev. A **65**, 042714 (2002).

[34] C. Cohen-Tannoudji, B. Diu, and F. Laloe, *Quantum Mechanics (Vols. I and II)* (Wiley, New York, 1978).

[35] A. Askar and A. S. Cakmak, J. Chem. Phys. **68**, 2794 (1978).

[36] C. Bena and G. Montambaux, New J. Phys. **11**, 095003 (2009).

[37] V. Krueckl and T. Kramer, New J. Phys. **11**, 093010 (2009).